International Journal of Thermal Sciences 182 (2022) 107790

Contents lists available at ScienceDirect

International Journal of Thermal Sciences

journal homepage: www.elsevier.com/locate/ijts

A computational conjugate heat transfer study of a rectangular minichannel undergoing sinusoidal flow pulsations

P.S. Kumavat [a,*], S. Alimohammadi [a,b], S.M. O'Shaughnessy [a]

[a] Department of Mechanical, Manufacturing and Biomedical Engineering, Trinity College, University of Dublin, Ireland
[b] School of Mechanical and Design Engineering, Technological University Dublin, Ireland

ARTICLE INFO

Keywords:
Pulsating flow
Minichannels
Hydrodynamic study
Heat transfer enhancement
Numerical analysis

ABSTRACT

The development of current and next generation high performance electronic devices has led to smaller components in more densely packed spaces. The increasing power levels have resulted in ever-increasing heat flux densities which necessitates the evolution of new liquid-based heat exchange technologies. Pulsating flow in single-phase cooling systems is viewed as a potential solution to the problems involving high heat flux densities. A review of published literature indicates a lack of time-resolved and space-resolved links between the hydrodynamic pulsating characteristics and associated heat transfer perturbations. The scope of this work involves the development of a validated three-dimensional conjugate heat transfer computational model to investigate hydrodynamically and thermally fully developed pulsating flows in a heated rectangular minichannel. Simulations were performed for a sinusoidal waveform with a fixed pulsation amplitude for varying pulsation frequencies in the range of 0.02 Hz to 25 Hz, corresponding to Womersley numbers in the range of $0.5 \leq Wo \leq 18.33$. Low pulsation frequencies exhibited the well known parabolic profile for the fluctuating hydrodynamic and thermal parameters, i.e., velocity, wall shear, and wall temperature. As a result, the axial pressure gradient, velocity, and wall shear stress profiles were in phase and similar results were obtained for the oscillating wall and bulk fluid temperatures. For the inertia dominated high frequency flows, an increase in axial pressure gradient leads to a phase lag of $\pi/2$ when compared with the velocity and wall shear profiles. The shorter time period pulsations exhibit unique attributes in the form of flow reversal effects at local near wall regions. High near wall thermal gradients were observed as a result of stronger viscous effects due to a narrowing thermal boundary layer; consequently the transverse diffusion of heat was ineffective. A phase lag and a subsequent drop in the peak magnitudes existed between the oscillating bulk and wall temperatures for high frequency flows. Fluctuations in near wall heat flux profiles showed a dependency on the imposed pulsation frequencies. For the chosen pulsation profile and frequencies, the overall time averaged thermal performance indicates that pulsating flow performs worse than steady flow for a flow rate amplitude of 1. The highest thermal performance was achieved for $Wo = 5.1$ while maintaining a low friction factor.

1. Introduction

The miniaturization of next-generation electronics packages and their associated high-power density circuits has created a need for innovative cooling solutions. Unsteady pulsating flow is viewed as a promising mechanism for augmenting heat transfer in single-phase forced convection cooling systems and could help to better regulate temperatures in applications involving high heat flux densities and/or those applications where fluid flow is restricted to confined spaces [1,2]. Although the phenomenon is commonly observed in biological processes such as arterial blood flow, pulsating flows may be particularly suited to areas such as electronics cooling and performance enhancement of heat exchangers. Impinging jet pulsating flows promoting flow instabilities and turbulence are viewed to be widely applicable for the cooling of turbine blades and de-icing of aircraft. With the advantages offered by high near wall velocity gradients resulting from flow pulsations, fouling deposits in stainless steel heat exchangers are seen to be effectively broken down which reduces thermal resistance. Due to the complexity of the coupled pulsating fluid flow and heat transfer and the wide range of pulsation formats that could be employed, a comprehensive parametric analysis of the phenomenon is considered to be of great interest.

Pulsating flows are distinct from oscillating flows as they have a non-zero mean mass flow rate, as shown in Fig. 1. The pulsating motion of the fluid intensifies the thermal and mass diffusion interactions with

* Corresponding author.
E-mail address: kumavatp@tcd.ie (P.S. Kumavat).

https://doi.org/10.1016/j.ijthermalsci.2022.107790
Received 26 October 2021; Received in revised form 27 June 2022; Accepted 30 June 2022
Available online 20 July 2022

Nomenclature

Greek symbols

η	Thermal performance, [–]
θ	Oscillatory phase, [rad]
λ	Pulsating time period, [s]
ν	Kinematic viscosity, [m^2/s]
ρ	Density, [kg/m^3]
σ	Darcy friction factor, [–]
τ	Bottom wall shear stress, [Pa]
χ	Axial displacement, [m]
ω	Angular velocity, [rad/s]

Latin letters

a	Channel width, [m]
Ar	Archimedes number, [–]
A_0	Flow rate amplitude, [–]
b	Channel height, [m]
c_p	Specific heat capacity, [J/kg·K]
D_h	Hydraulic diameter, [m]
f	Pulsation frequency, [Hz]
F_n	Dimensionless pulsation frequency, [–]
F_0	Dimensionless fluid displacement amplitude, [–]
g	Gravitational acceleration, [m/s^2]
Gr	Grashof number, [–]
h	Heat transfer coefficient, [$W/m^2 \cdot K$]
k	Thermal conductivity, [W/m·K]
L	Channel length, [m]
L_e	Hydrodynamic entry length, [m]
L_{th}	Thermal entry length, [m]
$\dot{m}$	Mass flow rate, [kg/s]
Nu	Nusselt number, [–]
p	Pressure, [Pa]
∇P	Pressure gradient, [Pa/m]
Pr	Prandtl number, [–]
Q	Flow rate, [m^3/s]
Ra	Rayleigh number, [–]
Re	Reynolds number, [–]
Re_{tot}	Total Reynolds number, [–]
Re_k	Kinetic Reynolds number, [–]
t	Time, [s]
T	Temperature, [K]
w	Foil thickness, [m]
Wo	Womersley number, [–]
x	Transverse coordinate direction, [m]
y	Vertical coordinate direction, [m]
z	Axial coordinate direction, [m]

Subscripts

b	Bulk fluid property
in	Channel inlet
max	Maximum value
m	Mean component
n	Normalized value
out	Channel outlet
p	Pulsating component
s	Steady component
w	Wall property

Other symbols

$\|A\|$	Space averaged component, [–]
$\bar{A}$	Time averaged component, [–]
A^*	Oscillating component, [–]

the boundary layer in contrast to steady flows. Several studies (e.g., [3–6]) have postulated a significant heat transfer enhancement while other studies report no or reduced heat transfer (e.g., [2,7,8]).

The characteristics of an unsteady pulsating flow are governed by the Womersley number, Wo, a dimensionless expression of the pulsating flow frequency in relation to viscous effects, and the dimensionless flow rate amplitude, A_0, which represents the ratio of the maximum oscillating flow rate (Q^*_{max}) to the cycle averaged flow rate (Q_s). These are defined in Eqs. (1) and (2) where D_h represents the hydraulic diameter, ω is the angular frequency of the oscillations, and ν is the kinematic viscosity of the fluid. The fluid displacement χ_m is defined wherein the fluid moves as a plug flow with a mean velocity u_m. Thus, the maximum fluid displacement χ_{max}, accounts for the maximum distance traversed by the driving pulse wherein $\chi_m = ((\chi_{max})/2)(1 - cos(\omega t))$. The dimensionless fluid displacement amplitude F_0 can be defined as the maximum fluid displacement divided by the hydraulic diameter.

$$Wo = (D_h/2)\sqrt{(\omega/\nu)} \tag{1}$$

$$A_0 = Q^*_{max}/Q_s \tag{2}$$

2. Previous studies

2.1. Hydrodynamics of flow pulsations

The effects of fluid perturbations and the associated augmentation or reduction of heat transfer due to unsteady pulsations have continued to be an active research area. Several researchers have explored the unsteady time and space dependent characteristics using analytical and/or experimental techniques. Early founding experimental studies in circular, ovular, and square cross-sections with laminar flows by Richardson [9] and Richardson and Tyler [10] visualized uniform a velocity distribution along the core regions and high near-wall velocity amplifications, establishing the phenomenon of "annular effects". Subsequently, several analytical studies reported this behaviour to be linked to oscillatory and/or pulsatory flows, such as studies by Holmes and Vermeulen [11], Harris et al. [12], Fan and Chao [13], for periodic pressure gradient imposed flow pulsations in ducts and pipes. Results for velocity profiles showed a resemblance to the experimental work of Refs. [9,10]. Analysing the effect of oscillatory flows in further detail theoretically, a founding study by Womersley [14] developed a relationship between the modulating flow amplitudes and the axial pressure gradient, indicating a phase-lag due to viscous drag effects. At low frequencies, the two were in phase, while at higher frequencies a consistent pressure gradient phase lag of up to $\pi/2$ existed with the flow rate amplitude decaying to a minimum.

Analytical solutions of the Navier–Stokes equations using Laplace transform and Fourier series approaches were described by Sexl [15] and Uchida [16] for an axial pressure gradient imposed unsteady flow superimposed by a mean steady flow. The phase differences between flow rate amplitudes, axial pressure gradient, and wall shear stress were explored for a range of frequencies, indicating the phenomenon as explored previously by Womersley [14]. Experimental observations by Lingford and Ryan [17] for $1.83 \leq Wo \leq 21.0$, and Denison and Stevenson [18] for $1.71 \leq Wo \leq 14.1$ using flow visualization

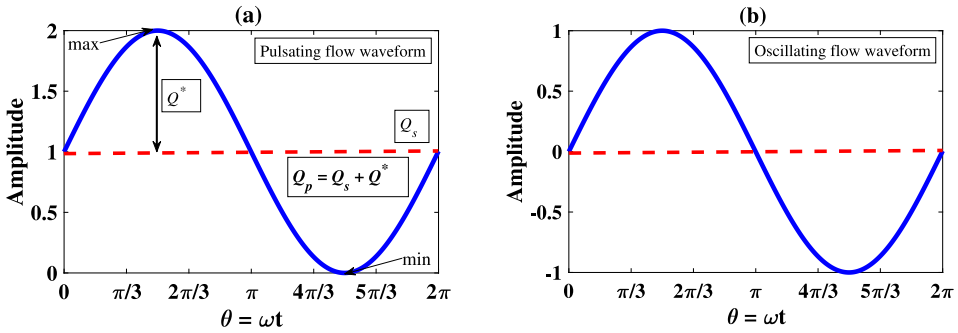

Fig. 1. (a) Pulsating flow waveform with non-zero mean mass flow (for a flow rate amplitude equal to 1), (b) and oscillating waveform with zero mean mass flow.

techniques for pulsating pipe flows also showed an agreement with the theory.

The distinguishable traits of quasi-steady, intermediate and inertia-dominated regimes in response to pulsating flows of different frequencies in channels were explored analytically by Haddad et al. [19] for $0.01 \leq Wo \leq 10$, followed by experimental investigations in pipe flows by Ünsal et al. [20], Durst et al. [21] for $0.8 \leq Wo \leq 6.6$ and Ohmi et al. [22] for $1.41 \leq Wo \leq 14.1$. For flow rate amplitudes equal to 1, such as in the current study, low frequency viscous dominated flows exhibited quasi-steady behaviour and the pulsating mass flow rate amplitude and axial pressure gradient were in phase with the parabolic velocity profiles. As the amplitude ratio dropped below one for the moderate-to-high frequency range, a phase lag was evident. Further in the higher frequency, inertia dominated regime, the phase delay approached $\pi/2$ as the amplitude ratio decayed to zero with minimal variation of velocity profiles in the channel core region. Prominent effects were observed in the near-wall regions leading to flow reversal.

Flow reversal resulting from high-frequency pulsating flows was explored by several recent studies, such as the analytical solution by Haddad et al. [19], and experimental investigations by Aygun and Aydin [23] and Blythman et al. [24]. Near wall and off-wall flow reversal effects were experimentally studied by Agyun and Aydin [23] for a wide frequency range of $1.07 \leq Wo \leq 402$ at a fixed flow rate amplitude of $A_0 = 0.48$ for a pipe flow. Blythman et al. [24] experimentally investigated a rectangular channel flow for $1.4 \leq Wo \leq 7$ and $A_0 = 0.9$ observing the near-wall flow reversal at inertia dominated high frequency using a combination of PIV and analytical solutions. The occurrence of flow reversal has a combined dependency on pulsation frequency, the inlet condition (pressure gradient vs. mass flow), and time. The reversal is viewed to be initiated from the near-wall regions and further propagates to the bulk fluid region due to the changing fluid direction, while the wall shearing stress tends to fade out where the velocity gradient falls to ≤ 0.

2.2. Heat transfer associated with flow pulsations

Early theoretical contributions to the molecular transfusion mechanism of an internal duct flow such as studies by Chatwin [25] and Taylor [26], discussed the combined action of axial heat transfer augmentation and fluid dispersion rate augmentation by transverse oscillation-induced diffusion. Large axial oscillating temperature gradients exist as a result. The transverse diffusion of heat and the mechanism of heat accumulation near the wall leading to an axial heat transfer enhancement under sinusoidal fluid motion were examined experimentally by Ozawa and Kawamoto [27] in a vertical tube arrangement for $7.1 \leq Wo \leq 23$. A coincidence of the thermal boundary layer thickness with the velocity boundary layer was observed from the phase delay between the fluid motion in the core and wall regions. Thus, heat transfer due to lateral heat diffusion was dominant due to a phase delay in temperature gradient and axial convection transport of bulk fluid induced by oscillations. Heat transfer was found to be enhanced by lateral heat diffusion due to a phase delay between the temperature gradient and axial convection. Subsequent studies of parallel plate channels by Sparrow and DeFaria [28], Seo et al. [29], and Siegal and Perlmutter [30], explored the heat diffusion mechanism between the imposed heated wall boundary and the bulk fluid under flow pulsations. An identical phase shift was observed for low frequencies, while for high frequency, fluctuations in the axial bulk temperature were seen to be insignificant compared to near wall temperature fluctuations. Local heat transfer was determined to be positive for most of the pulsation cycle wherein $T_w > T_b$ indicated that the heat flow was from wall to fluid. Both uniform wall temperature and uniform wall flux boundary conditions were investigated.

Several studies have reported significant heat transfer enhancement using pulsating flows. Liao et al. [3] in their analytical study for channel flows with uniformly heated wall reported a maximum achievable heat transfer enhancement of 200% for an oscillatory duct flow with water as the cooling medium using a uniformly heated wall with a Womersley number range of $0.1 \leq Wo \leq 2$. In an experimental study of pulsating flow in a minichannel heat sink by Persoons et al. [5], heat transfer enhancements of up 40% were achieved for pulsating Reynolds number amplitude in the range of $0.002 \leq Re_p/Re_s \leq 3$ with an operating frequency range of $6 \leq Wo \leq 17$. An analytical study by Moschandreou and Zamir [4] for pulsating flow through a tube under uniform wall heat flux predicted a heat transfer enhancement of 20% at a frequency corresponding to $Wo = 15$ and a flow rate amplitude of $A_0 = 1$, with a variation of Prandtl numbers between $0.5 \leq Pr \leq 5$. On the contrary, in a numerical study of pulsating pipe flows with an isothermal wall by Cho and Hyun [7] for Womersley number and pulsation amplitudes in the range $0 \leq Wo \leq 15$ and $0.01 \leq A_0 \leq 20$, a reduction in heat transfer compared to the steady flow was observed for the low and high extremes of frequency. This was attributed to a contrasting trend between the wall shear stress and heat transfer. It was seen that for moderate-to-high frequencies, heat transfer was reduced as the wall friction coefficient increased in magnitude.

Heat transfer performance is viewed to be dependent on the characteristics of the oscillatory motion of the fluid which leads to consistent disruptions to the development of the thermal boundary layer. The heat transfer is therefore viewed as being dependent on the pulsation waveform driving the flow e.g., sine, square, triangular. Yin and Ma analytically studied the effect of triangular waveforms in a uniformly heated capillary tube over a wide range of operating frequencies corresponding to $0.1 \leq Wo \leq 10$, and displacement amplitudes in the range $0.0001 \leq F_0 \leq 0.1$. A peak heat transfer enhancement of 24.5% was determined for a triangular waveform profile at $A_0 = 0.01$ and $Wo = 0.1$ compared with sinusoidal pulsations and a purely steady flow. An experimental study of pulsating flow in minichannels based on a square pulsation waveform performed by Mehta and Khandekar [2] over the Womersley number range $0.8 \leq Wo \leq 5.9$ found that the heat transfer was reduced compared to that obtained for steady flow. Using an analytical approach Blythman et al. [8] studied flow pulsations for a rectangular duct with two constant heat flux long walls for the

ranges $1.4 \leq Wo \leq 22.1$ and $0.0035 \leq F_0 \leq 8.77$. For high frequency pulsations, no notable transverse diffusion occurred as the temperature profiles were plug-like in the fluid core regions. For low frequencies, since the thermal diffusion time scale was shorter compared to the excitation period, heat diffused from the core region to the wall. Time dependent heat transfer was reduced in the first half-cycle and enhanced in the second half-cycle.

Recent studies involving modulation of excitation waveforms such as square, sawtooth, triangular and sinusoidal in microchannel heat sinks for frequencies $1 \leq f \leq 4.5$ using nanofluids by Xu et al. [31] have shown insignificant heat transfer for waveforms except square. With a considerable increase in pumping power and high flow frequency, the nanofluids indicated an enhancement in heat transfer of about 3.1% over pure water for a square waveform. In another microchannel study by McEvoy et al. [32] using PIV, the effects of flowrate modulations via asymmetric, triangular and sinusoidal flow pulsations for $1 \leq Wo \leq 5$ was studied. For the studied cases of conventional pulsation waveforms, an inconclusive heat transfer enhancement existed due to low impact on flow rate amplitudes, leading to an inefficient narrowing of the thermal boundary layer. The asymmetric flows showed intense fluid mixing with a rapid shift in flow velocity and corresponding pressure gradients led to an enhancement of up to 28% over steady. New works have also focussed on modifying the channel geometries such as by implementing grooved wall [33,34], sinusoidal wavy walls [35,36] or by incorporating surface roughness [37] to achieve promising heat transfer enhancement using pulsating flows. The introduction of recirculation zones and flow separation effectively disrupts the thermal boundary to enhance the mass momentum and thermal diffusion between wall and core, although with a sharp escalation in pressure gradient.

3. Research objectives

The potential heat transfer augmentation linked to flow pulsations has been explored by several studies in minichannels and pipes. Many of the approaches involve inspecting the underlying mechanics of pulsating and oscillating flows either in hydrodynamically or thermally developed flows. As per the authors' knowledge, limited parametric studies exist which elucidate the crucial link between the hydrodynamic pulsating characteristics and heat transfer perturbations.

The overarching goal of this study is to develop a validated numerical tool to evaluate the heat transfer performance of a heated minichannel in response to laminar pulsating flow throughput. This is achieved through numerical simulation of experimental conditions to identify the interlinked hydrodynamic-thermal characteristics of pulsed flow. The validated numerical tool will serve as a testbed for future investigations using different heating arrangements, pulsation formats, and flow conditions.

4. Numerical model

The numerical model is developed to closely replicate a parallel but separate experimental investigation of pulsed flow in a rectangular minichannel. Fig. 2 provides a schematic of the geometric model and computational domain. A rectangular duct of aspect ratio = 14.3 with internal dimensions of 345 mm × 20 mm × 1.40125 mm (length × width × height) is modelled to perform a three-dimensional conjugate heat transfer study. The height here is inclusive of the fluid domain plus a solid domain equivalent to an Inconel foil of thickness 12.5 μm as used in the parallel experiment, reported by Kumavat et al. [38,39].

4.1. Numerical model formulation

Simulations are performed by discretizing and linearizing the mass, momentum, and energy conservation equations using ANSYS CFX 2020 R2 which is based on the finite volume method. CFX follows a vertex-centred approach, thus the solution variables are stored in the mesh vertices (nodes). The model includes the following assumptions:

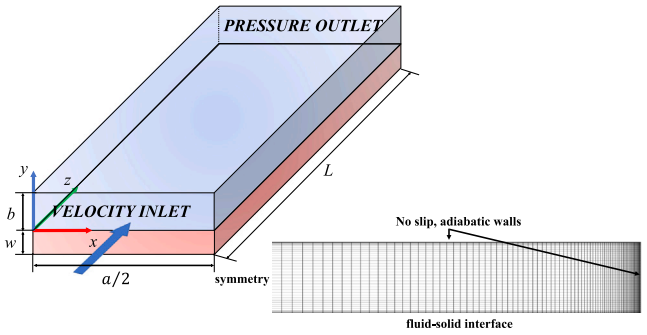

Fig. 2. Computational domain and boundary conditions. Inset view shows the finely resolved mesh of the fluid domain. The solid domain is a volumetric heat source of 3×10^6 W/m^3.

i. The working fluid (water) is incompressible.
ii. The flow is laminar with no viscous dissipation (heating) effects.
iii. Uniform conditions exist at the inlet and a zero gradient boundary condition is imposed at the outlet.
iv. The influence of body forces (i.e., gravity) is negligible.
v. The thermo-physical properties of both the fluid and solid are invariable with temperature.
vi. Radiation heat losses are negligible.
vii. The flow and heat transfer are symmetric about the minichannel mid-plane of the transverse direction (x).

Regarding assumption (ii), the Womersley number range is $0.5 \leq Wo \leq 18.33$ and the steady and maximum pulsating Reynolds numbers are $Re_s = (U_m D_h)/\nu = 163$ and $Re_{p,max} = U_{z,max} D_h/\nu = 326$ respectively, thus a laminar flow approximation with no viscous heating is reasonable. Although assumption (iii) is not physically realistic, a sufficiently long channel is modelled to allow for the hydrodynamic (~19 mm) and thermal (~116 mm) entrance lengths which are calculated using Eqs. (3) and (4) according to Refs. [40,41] and verified by assessing the relevant profiles resulting from the simulations. Regarding assumption (iv), gravity acts perpendicular to the flow and the maximum Archimedes number $Ar = Gr/Re_{tot}^2$ is $(6.1 \times 10^{-3}) \ll 1$, thus natural convection heat transfer will be dominated by forced convection. Simulations were performed with gravitational forces and buoyancy included via the Boussinesq approximation [42] but no significant change in results was determined. The maximum temperature range in this investigation is 295 K to 313 K, such that assumptions (v) and (vi) are deemed reasonable. Regarding assumption (vii), several previous studies of low Reynolds number pulsating flows have predicted or shown symmetry in the velocity, pressure and temperature distributions, such as studies by [8,13,18,30]. The application of the symmetry condition significantly reduces computational effort and enables the necessary mesh refinement and was hence deemed appropriate for the current study.

$$\frac{L_e}{D_h} = [(0.631)^{1.6} + (0.0442 Re_s)^{1.6}]^{1/1.6} \tag{3}$$

$$L_{th} = Pr \times L_e \tag{4}$$

The governing (fluid) equations of the conservation of mass, momentum and energy are expressed in incompressible form as follows:

$$\nabla \cdot \mathbf{u} = 0 \tag{5}$$

$$\frac{\partial \mathbf{u}}{\partial t} + (\mathbf{u} \cdot \nabla)\mathbf{u} = -\nabla w + \nu \nabla^2 \mathbf{u} + \mathbf{g} \tag{6}$$

$$\rho c_p [\frac{\partial T}{\partial t} + (\mathbf{u} \cdot \nabla) T] = k \nabla^2 T + S \tag{7}$$

where $\boldsymbol{u}$, T represent the velocity and temperature fields, and ρ, ν, k, c_p are the density, kinematic viscosity, thermal conductivity and specific heat of the fluid, respectively. $\boldsymbol{g}$ represents gravitational acceleration

and w represents the specific work ($= p/\rho$), where p is the pressure. S represents the volumetric heat generation. Boldface variables represent vector quantities. Eq. (7) is easily manipulated for application to the solid phase.

4.2. Boundary conditions

For steady flow simulations, the minichannel inlet condition is a constant velocity of $U_z = 0.013$ m/s at a temperature of 293 K. This temperature represents the approximate room temperature for the associated experiment. For pulsating flow, the same temperature condition is used but the inlet velocity is implemented with a user defined function (UDF) according to the following expression:

$$U_z = U_s + U^*_{max} sin(2\pi f t) \tag{8}$$

In the above equation, U_z is the inlet velocity along the axial (z) direction while the U_x and U_y components are equal to 0 m/s. U_s is the steady flow velocity and U^*_{max} is the peak oscillatory velocity, f is the pulsating frequency, and t is time. At the outlet, the pressure outlet boundary condition is applied with a gauge pressure of 0 Pa and atmospheric or operating pressure of 101 325 Pa. The no-slip velocity condition is applied to all walls. The top and side walls are treated as adiabatic and the bottom wall of the minichannel (fluid domain) is formed by a heated solid domain which is defined with a volumetric heat source of 3×10^6 W/m^3. The bottom heated solid domain simulates Inconel 600 foil material (12.5 μm thickness) specified with a density of 8420 kg/m^3, specific heat capacity of 444 J/kg · K, and thermal conductivity of 14.9 W/m·K. The working fluid is water with a density of 1000 kg/m^3, dynamic viscosity 8×10^{-4} Pa · s, specific heat capacity of 4137.9 J/kg · K and thermal conductivity of 0.60 W/m · K.

4.3. Simulation specification

The generated grid as seen in Fig. 2 is a structured hexahedral mesh, refined at entry regions and wall boundaries to capture the near wall gradients. A coupled solver is used to reduce the number of iterations required, and adaptive time stepping is used to maintain low Courant–Friedrichs–Lewy numbers (typically CFL < 5). Since CFX is an implicit solver, the role of the CFL number in convergence is not as crucial as that for some explicit solvers [43]. A second order upwind spatial discretization scheme is chosen for the convective terms of the momentum and energy equations. Diffusion terms are calculated by the solver based on element shape functions and are second order accurate. The pressure term is corrected by applying a fourth order correction term thus preventing pressure–velocity decoupling. To achieve high computational accuracy and obtain solution boundedness, a high-resolution advection scheme is preferred as it reduces numerical instability to a minimum by maintaining second order accuracy of gradients. A RMS scaled residual value of $< 10^{-5}$ is used as a convergence criterion for the governing equations. Additionally, other parameters, e.g., inlet and outlet mass flow rate, are tracked to judge the convergence of the simulations.

4.4. Parameter interpretation

The minichannel dimensions are defined with length (L) = 345 mm, width (a) = 20 mm, and height (b) = 1.4 mm. The hydraulic diameter of the rectangular minichannel (D_h) is defined as:

$$D_h = \frac{2ab}{a+b} \tag{9}$$

To determine and evaluate the thermal performance of heated minichannels under pulsating inlet conditions, convective heat transfer parameters are introduced. The time averaged Nusselt Number ($\bar{Nu}$) as given by Eq. (10) defines the relationship between the fluid thermal conductivity and the surface convective heat transfer rate, averaged over one pulsation cycle (λ), and requires estimation of the time-averaged heat transfer coefficient ($\bar{h}$) as given by Eq. (11), wherein ($|\bar{q_w}|$) is the time–space averaged bottom wall heat flux. ($\bar{T_w}$) is the time-averaged heated wall temperature in the fully developed region. ($\bar{T_b}$) is the time-averaged bulk fluid temperature as given by Eq. (13) [33]. ($|T_w|$), ($|T_{in}|$) and ($|T_{out}|$) are instantaneous spatial-averaged temperatures at the wall, channel inlet ($z = 0$), and channel outlet ($z = 0.345$ m), respectively. The normalized enhancement of heat transfer compared to steady flow only is described by Eq. (14), where (Nu_s) represents the steady flow Nusselt number. To characterize the performance of sinusoidal flow pulsations simultaneously in terms of heat transfer and pressure drop, a thermal performance parameter (η) is defined as given in Eq. (15). The time averaged friction factor for pulsating flow ($\bar{\sigma_p}$) is obtained from Darcy–Weisbach equation [44], described in Eq. (16) where (ΔP) is the pressure drop. (σ_s) is the corresponding friction factor for steady flow at the same Reynolds number (Re).

$$\bar{Nu} = \frac{\bar{h} D_h}{k} \tag{10}$$

$$\bar{h} = \frac{|\bar{q_w}|}{\bar{T_w} - \bar{T_b}} \tag{11}$$

$$\bar{T_w}(or \bar{q_w}) = \frac{1}{\lambda}\int_0^{\lambda} |T_w(or q_w)| dt \tag{12}$$

$$\bar{T_b} = \frac{1}{\lambda}\int_0^{\lambda} \frac{(|T_{in}| + |T_{out}|)}{2} dt \tag{13}$$

$$dNu = \frac{\bar{Nu} - Nu_s}{Nu_s} \tag{14}$$

$$\eta = \left(\frac{\bar{Nu}}{Nu_s}\right).\left(\frac{\bar{\sigma_p}}{\sigma_s}\right)^{-1/3} \tag{15}$$

$$\bar{\sigma_p} = \frac{1}{\lambda}\int_0^{\lambda} \frac{2(\Delta P/L) D_h}{\rho U_s^2} dt \tag{16}$$

4.5. Numerical model verification

Solution errors in the form of numerical diffusion or truncation are associated with the chosen grid discretization schemes. A discrepancy in the numerical results between the asymptotic value and true physical solution prevails. Thus, a threshold is to be established below which the solution is recognized to be independent of the mesh resolution [43]. Verification study by evaluating the mesh independence and the consistency of results requires quantification of discretization and truncation errors [45]. A method of analysing grid convergence is suggested by Celik et al. [46], as recommended by the *ASME Journal of Fluids Engineering*. The advantage of this technique is that successively doubling the grid resolution to obtain a finely resolved grid is unnecessary.

The Grid Convergence Index (GCI) is a measure of percentage error which provides a confidence bound around the estimated error signifying the estimation of numerical model uncertainty. Characteristically, three different sets of grids are used for this technique to compute the range of solution convergence and accordingly predict the modification using enhanced grid refinement. Grid independence studies were carried out according to Table 1. Sample plots are provided in Figs. 3 and 4. Three grids sizes are generated using ANSYS meshing, with 1 718 669 cells considered as the fine grid, 622 504 cells as the medium grid, and 206 005 cells as the coarse grid. Some results obtained from the three grids for derived parameters such as axial pressure gradient, wall shear stress, time averaged Nusselt number, and time averaged friction factor are presented in Table 1. The difference in solution parameter values between the medium and coarse grids and the reference fine grid is low. For example, time averaged Nusselt numbers are almost identical and the trend in transient wall shear stress indicates oscillatory convergence behaviour. The maximum numerical uncertainty for the three grids shown in Table 1 indicate that the solutions are within the asymptotic range of convergence. The global order of accuracy for fine grid size is 1.15 as oscillatory convergence occurs at 75% of the grid points

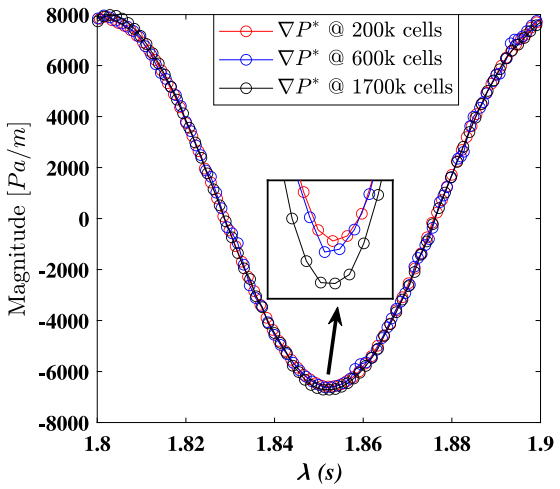

Fig. 3. Oscillating axial pressure gradient for one pulsation cycle for different mesh densities at a frequency of 10 Hz ($Wo = 11.5$). Fine grid numerical uncertainty is about 1.3%.

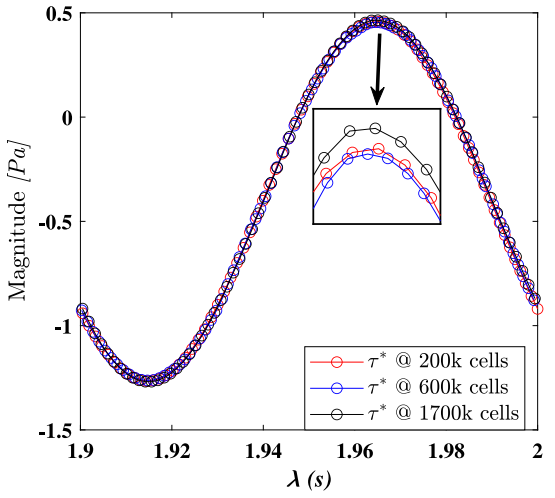

Fig. 4. Oscillating bottom wall shear stress for one pulsation cycle for different mesh densities at a frequency of 10 Hz ($Wo = 11.5$).

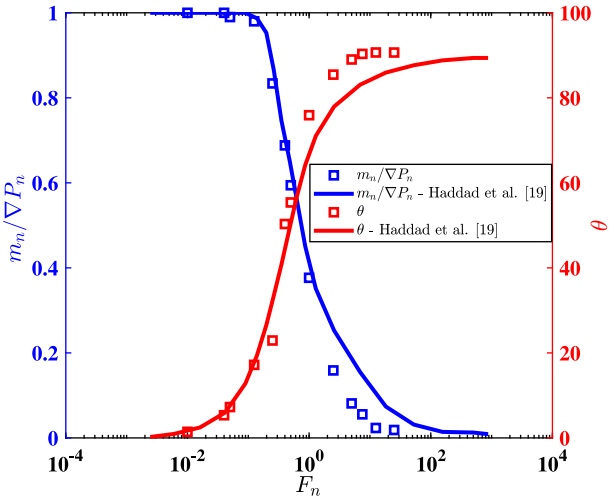

Fig. 5. Variation of normalized mass flow rate amplitudes with respect to the normalized axial pressure gradient and the associated phase differences as a function of dimensionless frequency ($F_n = f * (a^2/\nu)$). Symbols represent the current study, while lines represents analytical solution from Haddad et al. [19].

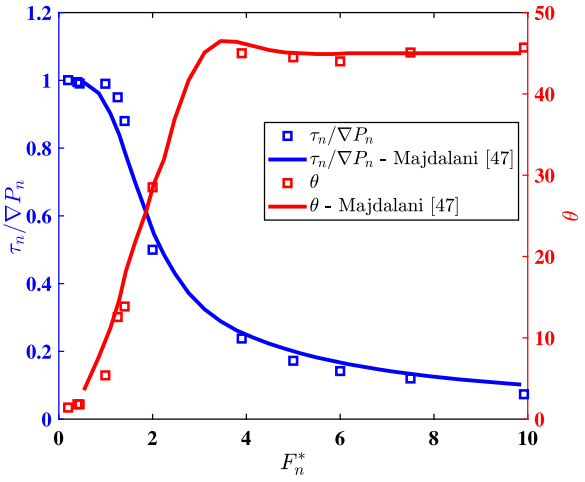

Fig. 6. Variation of normalized wall shearing stress with respect to normalized axial pressure gradient and the phase differences as a function of dimensionless frequency ($F_n^* = \sqrt{Re_k}$). Symbols represent current numerical study, while lines represent analytical solution for a channel flow from Majdalani [47].

Table 1
Selected results from mesh independence study for $Wo = 11.5$.

	Coarse	Medium	Fine
Refinement factor	1	3	2.83
Cell count	2×10^5	6×10^5	1.7×10^6
∇P_{min} [Pa/m]	−6588.9	−6620.7	−6711.1
(% deviation)	(1.82)	(1.35)	(–)
τ_{max} [Pa]	0.4568	0.4548	0.4645
(% deviation)	(1.66)	(2.10)	(–)
$\bar{Nu}$	5.0834	5.0826	5.0811
(% deviation)	(0.045)	(0.029)	(–)
$\bar{\sigma_p}$	0.813	0.815	0.818
(% deviation)	(0.61)	(0.36)	(–)
GCI_{max} (%)	–	–	1.3

shown in Figs. 3 and 4. Thus, the fine grid with an acceptable GCI factor is the preferred mesh for the study, which yields an acceptable level of accuracy and performance with respect to computational time. Discretization error bars for the fine grid solution are not shown in the figures for clarity.

4.6. Numerical model validation

Validation of the computational model is carried out by comparing results against established studies of sinusoidal pulsating flow in channels from Haddad et al. [19] and Majdalani [47], as shown in Figs. 5 and 6. Mass flow rate imposed pulsations in the fully developed region was studied analytically by Haddad et al. [19] using a Fourier series method. The deviation of results at higher frequencies (maximum deviation of 5%) observed in Fig. 5 is reasonable considering the disparity in the modelling characteristics adopted, i.e., two-dimensional analytical predictions versus a three-dimensional finite volume method conjugate heat transfer model. Pressure gradient imposed flow pulsations were investigated by Majdalani [47] using a Fourier series approximation. The results presented in Fig. 6 for wall shear amplitudes and phase angles relative to the axial pressure gradient indicate a good agreement (maximum deviation of 3%) with each other.

5. Results and discussions

5.1. Hydrodynamic profiles

Four different sinusoidal pulsating frequencies of 0.02 Hz, 0.5 Hz, 2 Hz and 25 Hz are studied, corresponding to Womersley numbers of

0.5, 2.5, 5.1 and 18.3, respectively. A flow rate amplitude of A_0 = 1 is maintained constant throughout the study. The data presented is investigated from the hydrodynamically and thermally fully developed region of the minichannel.

Fig. 7 presents the temporal evolution of the volumetric flow rate ratio (Q^*/Q_s), axial pressure gradient ratio ($\nabla P^*/\nabla P_s$) and the bottom wall ($y = 0$) shear stress ratio (τ^*/τ_s) in response to sinusoidal flow pulsation. The pressure gradient is measured as per unit length difference between the inlet gauge pressure and the local pressure at the fully developed sampling region ($z = 0.3$ m). For low to moderate frequency viscous dominated flows, the time scales of fluid displacement are longer, thus the wall shear stress and axial pressure gradient are in phase with the flow rate. For $Wo = 2.5$, the peak ∇P_p = 1261.2 Pa/m. As the pulsation frequency is increased, it results in rapid fluctuations in the fluid displacement time scales. This effect leads to a subsequent increase in the axial pressure gradient, which attains a maximum value of ∇P_p = 18 040.9 Pa/m for $Wo = 18.3$ caused by the inertia dominated core fluid region. This phenomenon was introduced by Womersley [14] for a constant axial pressure gradient and varying flow rate in a cylinder. A confluence of wall shear stress and axial pressure gradient as a factor of varying pulsation frequency was established by Uchida [48]. Similar behaviour was experimentally demonstrated by Ojha et al. [49] and Ünsal et al. [20].

Distinct features of flow pulsations were established by Richardson and Tyler [10] in their experimental study of flow pulsations in ducts. Similarly by Harris et al. [12] in their flow visualization investigations of oscillating flow in tubes, and Fan and Chao [13] using theoretical predictions of pulsating flows in ducts. Conventional parabolic velocity profiles are present for flows with $Wo < 1$ and annular effects exist with peak velocity near the channel walls for flows with $Wo > 1$. The oscillating velocity, i.e., the pulsating component minus the time averaged component, (at $y = 0.0007$ m & $z = 0.3$ m) and the oscillating shear stress (at $y = 0$ m & $z = 0.3$ m) profiles in the transverse (x) direction are shown for a range of pulsation frequencies in Figs. 8 and 9. In the case of low to moderate flow pulsations, the observed velocity and wall shear stress profiles are similar. As viscous forces are predominant closer to the wall regions, low amplitudes of near wall (0.008 m $\leq x \leq 0.01$ m) velocity are observed at these frequencies. For higher frequencies, the wall viscous effects tend to be stronger as is seen from Fig. 9(c) and (d), thus indicating higher near wall (0.008 m $\leq x \leq 0.01$ m) shear stress amplitudes with a peak value of $\tau^* = 2.3$ Pa for $Wo = 18.3$ as a result of the increased near-wall (0.008 m $\leq x \leq 0.01$ m) velocity gradients.

Fig. 11 plots the axial velocity profile at different phases for one complete pulsation cycle. Low frequency behaviour indicates a typical parabolic velocity profile as has been previously reported in Refs. [10,11,17,48]. While for the high frequency plot ($Wo = 18.3$) in Fig. 11(b), local near wall (0 mm $\leq y \leq 0.2$ mm and 1.2 mm $\leq y \leq 1.4$ mm) flow reversal effects are noticed for phases $\pi - 1.4\pi$ during the backward stroke. This phenomenon is also evident from the axial velocity contour and vectors in the near-wall regions illustrated in Fig. 10 at phase angles π and $3\pi/2$ for $Wo = 18.3$. The predominant bulk inertia in the streamwise direction acts to perturb the near wall shear region. This rapid withdrawal of flow rate occurs as a special feature of pulsating flows and is observed for high frequencies and high kinetic Reynolds number Re_k (defined as the square of Womersley number) for a fixed ratio $A_0 = 1$, reported by Muntges and Majdalani [50]. The complex nature of flow reversal effects has been described based on analysis of near wall and off wall reversals for pipe and parallel channel flows by Haddad et al. [19] who established its occurrence to be purely dependent on the pulsation frequency, flow rate amplitude and time instants of the cycle. Similar behaviour has been reported in recent time-dependent experimental studies by Aygun and Aydin [23] for high frequency pipe flows (Wo = 105, 226, 403). Blythman et al. [24] experimentally and analytically observed near wall flow reversal effects for channel flows at $Wo = 7.0$.

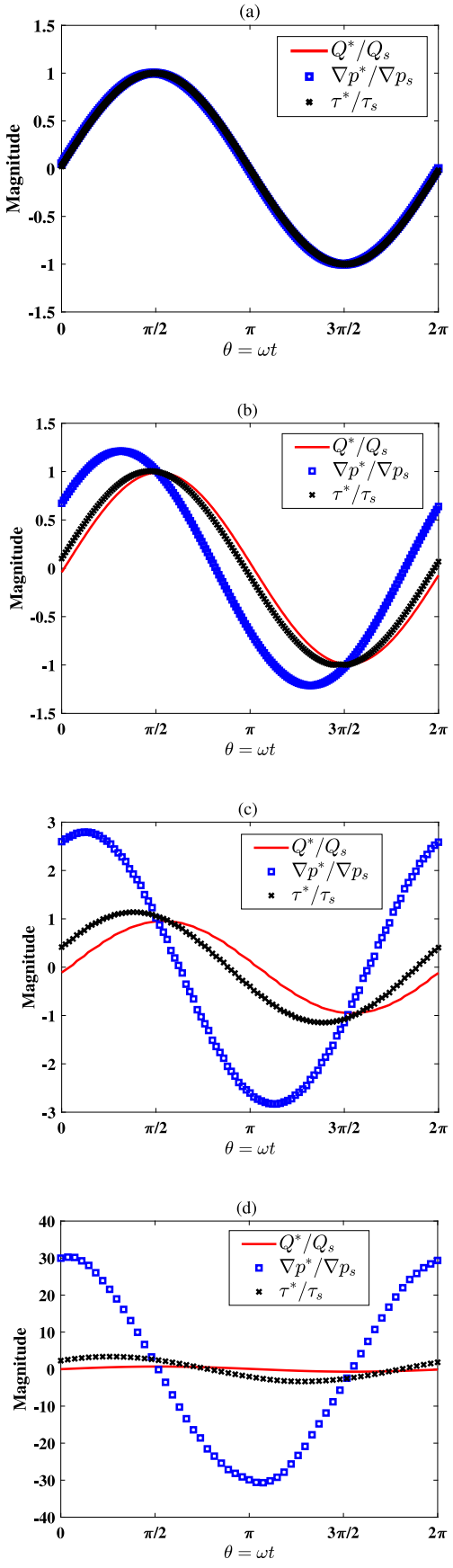

Fig. 7. Temporal evolution of normalized flow rate, wall shear stress and pressure gradient for a fixed $A_0 = 1$ and frequency (a) $Wo = 0.5$, (b) $Wo = 2.5$, (c) $Wo = 5.1$ and (d) $Wo = 18.3$.

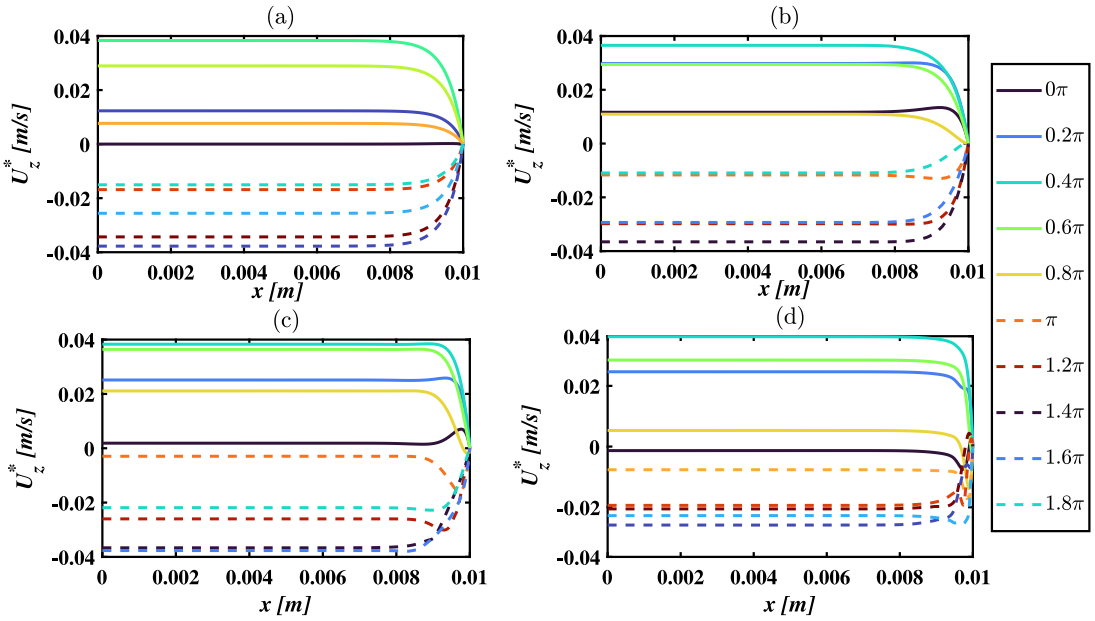

Fig. 8. Instantaneous oscillating axial velocity profiles at (y = 0.0007 m, z = 0.3 m) along the transverse direction for (a) Wo = 0.5, (b) Wo = 2.5, (c) Wo = 5.1 and (d) Wo = 18.3.

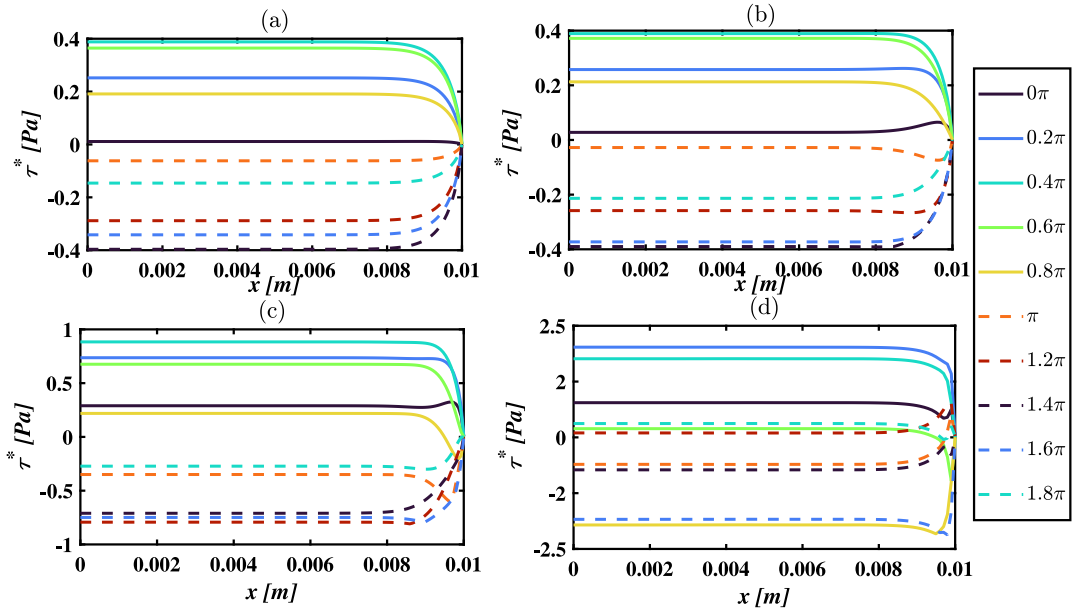

Fig. 9. Instantaneous oscillating wall shear stress profiles (at y = 0, z = 0.3 m) along the transverse direction for (a) Wo = 0.5, (b) Wo = 2.5, (c) Wo = 5.1 and (d) Wo = 18.3.

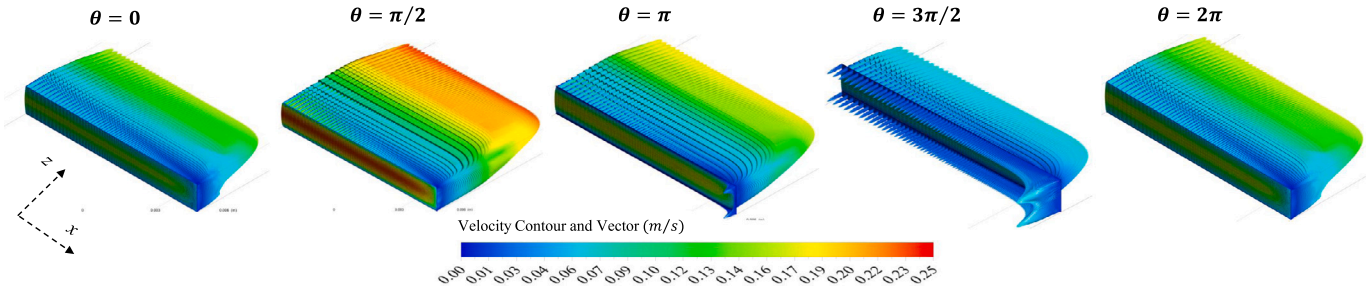

Fig. 10. Axial velocity contours and vectors at equal phase intervals of a cycle for Wo = 18.3 in the fully developed regime across the transverse direction.

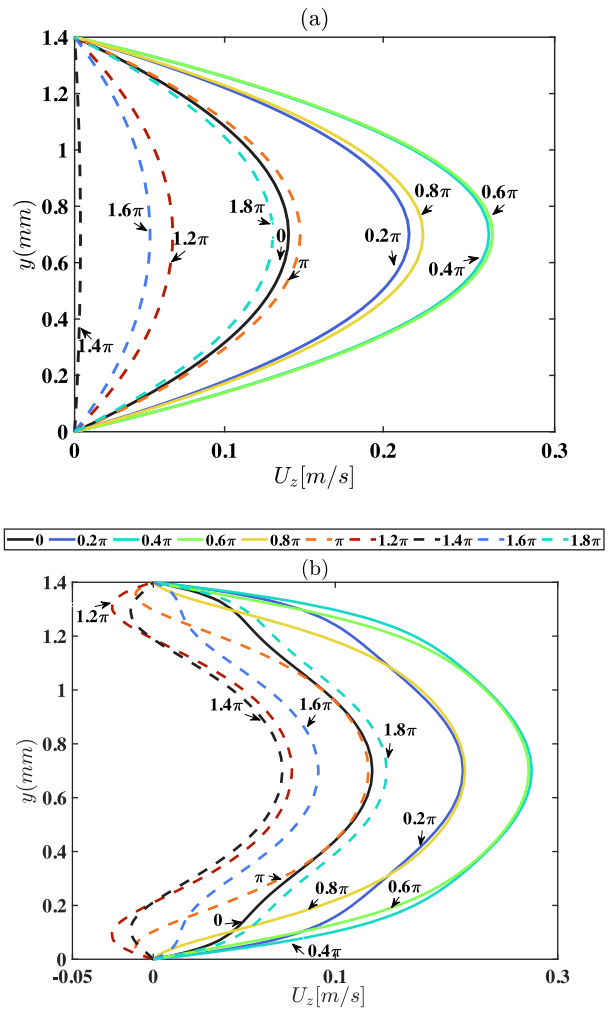

Fig. 11. Fully developed axial velocity profiles at the symmetry plane for two distinct frequencies (a) Wo = 0.5 and (b) Wo = 18.3.

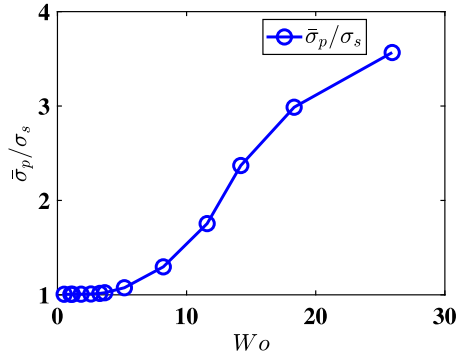

Fig. 12. Effect of friction factor ratio on dimensionless pulsating frequency Wo.

Fig. 12 plots the friction factor ratio ($\bar{\sigma}_p/\sigma_s$) vs. Womersley number. At low frequencies, the ratio is approximately equal to 1, indicating little effect of pulsation on the friction factor. Whereas for higher frequencies ($Wo \geq 5$) the increasing wall stresses result in a sharp rise in the friction factor ratio.

5.2. Thermal profiles

For an oscillatory fluid under a thermal gradient, the time scales of axial convection and transverse diffusion determine the heat transfer enhancement guided by an imposed flow frequency. It is understood that the core bulk fluid drives the heat flow within fluid boundary layers during the first half of the pulsation cycle. During the second half of the pulsation cycle, transverse diffusion of heat occurs from the walls to core fluid regions due to high near-wall viscous effects. The rate of heat transfer augmentation is dependent on the optimal excitation frequency.

Fig. 13 shows the time-dependent oscillating wall temperature at y = 0 m & z = 0.3 m along the transverse direction (x). For low pulsation frequencies Wo = 0.5 and Wo = 2.5 a significant amount of heat is diffused to the fluid from the heated wall since thermal diffusion time scales are shorter in comparison to the longer pulsation period. This eventually increases the fluid temperature. At high frequencies, convection heat transfer remains dominant while the pulsation periods are shorter. Due to flatter temperature profiles in the fluid core region, the transverse thermal diffusion is ineffective. Smaller magnitudes of near side wall ($0.008 \leq x \leq 0.01$) peaks are observed for moderate to high frequencies (e.g., T_w^* = 0.0024 °[C] for Wo = 18.3) as shown in Fig. 13(c) and (d) indicating steep near-wall thermal gradients due to the influence of greater viscous effects in the fluid. Similar effects were observed in the velocity and wall shear profiles in Figs. 8 and 9. The influence of near side-wall viscous effects are evident from Fig. 14 which shows the temperature contours in the fluid domain in the thermally fully developed region for a predominantly viscous flow of Wo = 2.5 at five distinct phase intervals. Large thermal gradients exists for all the phases of the pulsating cycle in the region where the bottom heated wall meets the side-wall. The time-dependent behaviour of the oscillating wall temperature and bulk temperature as presented in Fig. 15 shows a clear influence of pulsation. The effects of wall thermal inertia for pulsating channel flows have been shown to be a contributing factor to large temperature gradients in core and wall regions [51]. There exists a phase lag between the bulk and wall temperatures, which is evident for high frequency flow pulsations because of shorter net fluid displacement timescales, leading to a corresponding reduction in magnitude of wall and bulk temperatures.

The difference in Nusselt number (see Fig. 16) indicates an increasing trend with an increase in frequency. The fluid pulsation parameters exhibit an interdependence on the heat transfer due to a time-varying velocity profile, temperature profile, and wall thermal inertial effects [50]. The results presented here are in agreement with the analytical trends established for a sinusoidal pulsatile channel flow by Yuan et al. [51] and for a pipe flow by Hemida et al. [52]. The difference in Nusselt number is described to be always negative overall. This difference reaches zero at higher pulsation frequencies since the flow exhibits a quasi-steady behaviour. The largest difference in Nusselt number for the current study is considerably small, less than 0.4% of the steady value (Nu_s = 5.0825).

A pulsating flow rate modulation study by Brereton and Jiang [53] for pipe flows reported similar trends for the time averaged heat transfer, with a reduction of 0.1% for Wo = 2.5, A_0 = 2 and Pr = 7 for a positive-leading flow profile. Experimental investigations of square flow pulsations by Mehta and Khandekar [2] indicated only a marginal enhancement for Wo = 3.4 and 5.9 while more widely a reduction in heat transfer was observed. A theoretical analysis by Yuan et al. [51] reported a significant reduction in Nusselt number for sinusoidal pulsations in a channel, with up to 10% deterioration compared with steady flow for Wo = 0.5, A_0 = 1.5 and Pr = 1.5. An analytical study by Blythman et al. [8] of sinusoidal flow pulsations in a channel imposed with four heated walls reported deterioration in heat transfer of up to 0.8% for A_0 = 0.375 at Wo = 1.4 and Pr = 1. Thus, the enhancement and deterioration of mean Nusselt number

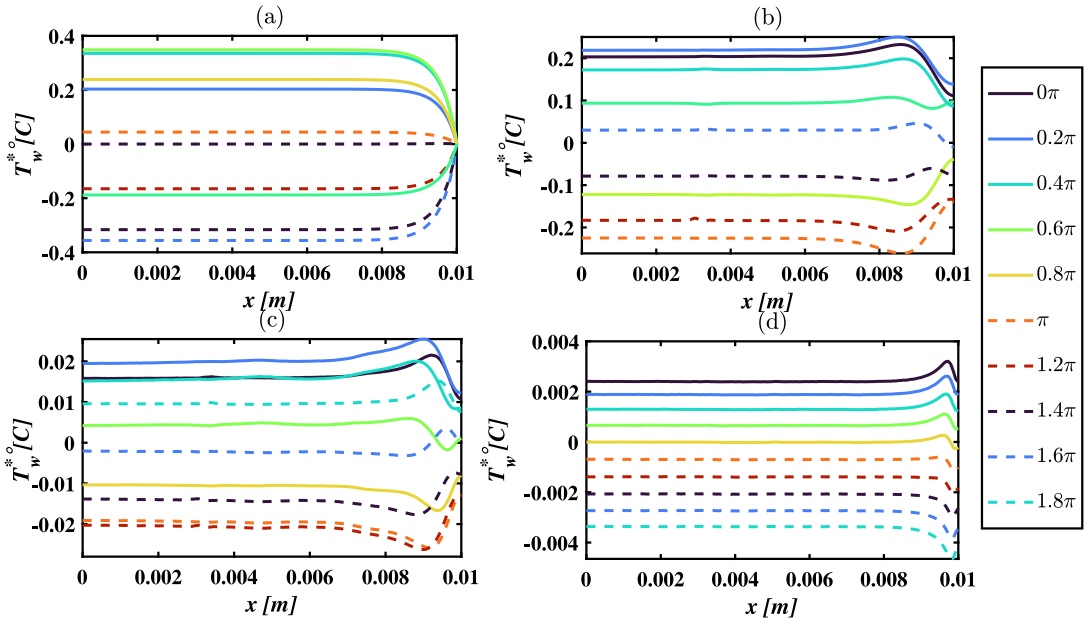

Fig. 13. Instantaneous oscillating wall temperature profiles (at $y = 0$, $z = 0.3$ m) along the transverse direction for (a) $Wo = 0.5$, (b) $Wo = 2.5$, (c) $Wo = 5.1$ and (d) $Wo = 18.3$.

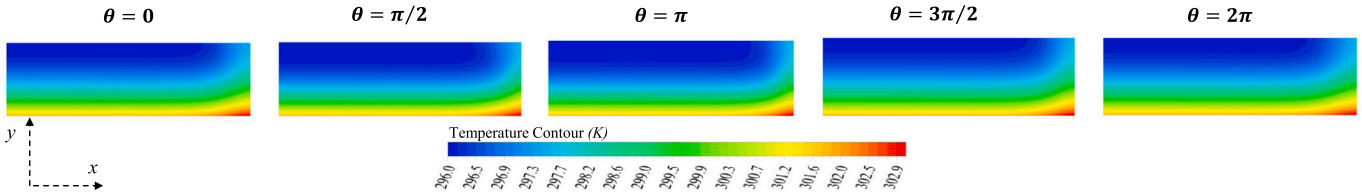

Fig. 14. Fluid domain temperature contours at equal phase intervals of a cycle for $Wo = 2.5$ in the fully developed regime (at $z = 0.3$ m) across the transverse direction.

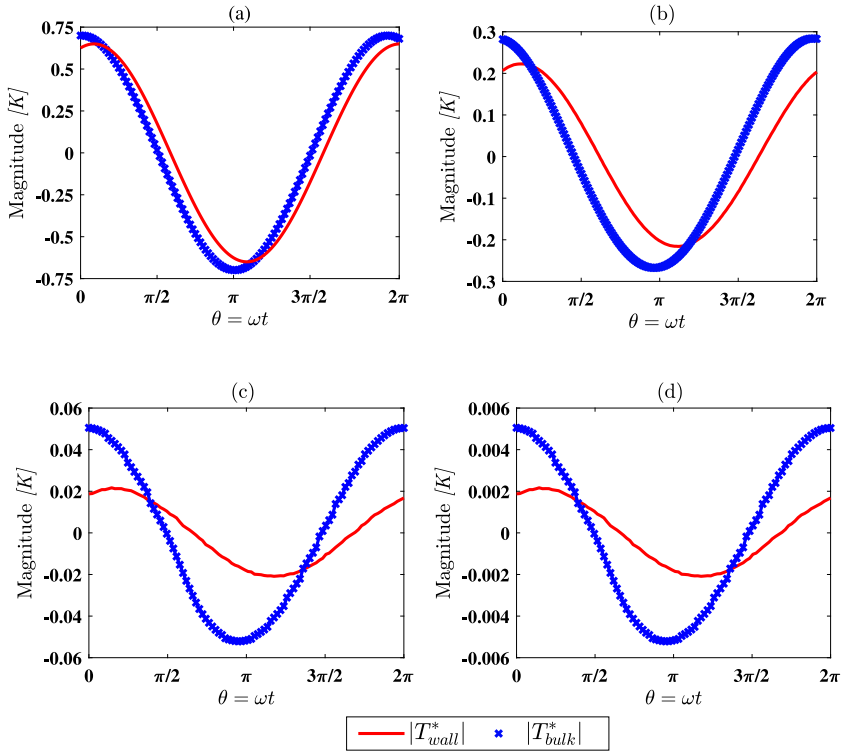

Fig. 15. Temporal variation of the spatially averaged oscillating wall and bulk fluid temperatures for (a) $Wo = 0.5$, (b) $Wo = 2.5$, (c) $Wo = 5.1$ and (d) $Wo = 18.3$.

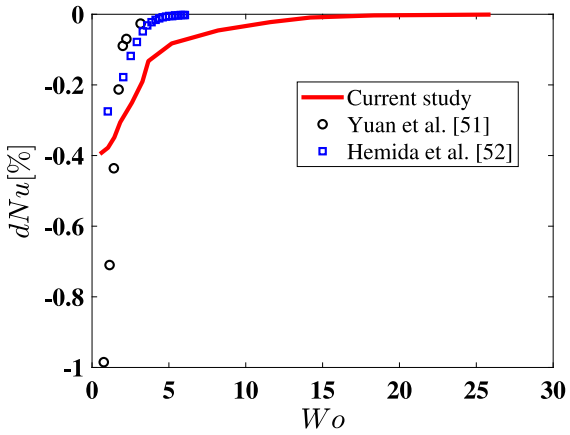

Fig. 16. Difference in Nusselt number as a factor of pulsation frequency. Symbols represent literature studies by Yuan et al. [51] ($Pr = 1.5$, $A_0 = 1$, thermally developed), Hemida et al. [52] ($Pr = 5$, $A_0 = 1$, thermally developing).

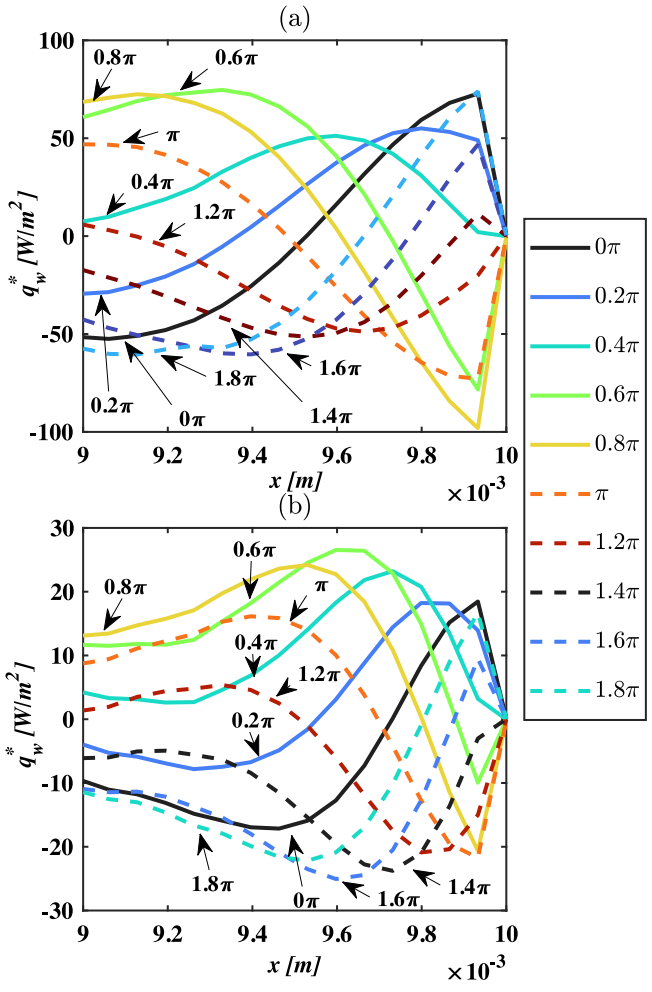

Fig. 17. Oscillating transverse bottom wall (at $y = 0$ and $z = 0.3$ m) heat flux profiles in the region near the side wall of the channel, for (a) $Wo = 2.5$, (b) $Wo = 5.1$.

are conditional and dependent on the excitation waveform and flow parameters.

The oscillating wall heat flux profiles (at $y = 0$ m & $z = 0.3$ m) shown in Fig. 17 describe the effect of heat diffusion from the heated wall to the fluid as the fluid convective time scales are shortened for low

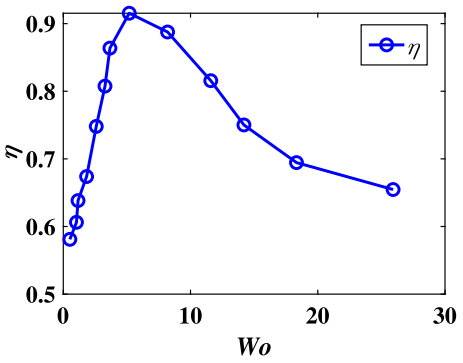

Fig. 18. Thermal performance evaluation with varying dimensionless pulsation frequencies Wo.

to high frequency pulsations. As a result, the low frequencies indicate larger near wall (0.009 m $\leq x \leq 0.01$ m) heat flux oscillations of about 70 W/m^2 whereas for higher frequencies the magnitudes are reduced to ~12 W/m^2 signifying that the flow tends to behave like a steady flow and the effects of heat diffusion are dampened out with an increase in pulsation frequency. The crucial interdependence of the thermal time scales and the fluid convective and excitation time scales affects the local as well as global time–space averaged Nusselt number. Fig. 18 plots the overall thermal performance, as defined by Eq. (15), of a sinusoidal flow rate pulsation for varying frequencies. It is noted that the thermal performance η is < 1 for the studied parameter space. This is due to the symmetric characteristics represented by a sinusoidal pulse which tends to attain a quasi-equilibrium with the cyclic process of removal and retention of heat in the channel. The highest thermal performance was obtained for $Wo = 5.1$ which is as a result of a lower friction factor. The low frequency flows $Wo \leq 3$ exhibit a diminishing impact on the heat transfer as is also noticed from Fig. 16 although with low values of friction factor. Whereas, for moderate–high frequency flows $Wo \geq 5$, potential enhancements in heat transfer are likely to exist at higher flow rate amplitudes.

6. Conclusion

A three-dimensional numerical conjugate heat transfer model was developed to investigate laminar pulsating flow in a rectangular minichannel with a bottom heated wall. This study provides a crucial link between the flow and thermal characteristics that dictate pulsating laminar flow convective heat transfer. Simulations were performed with symmetric sinusoidal pulsation waveforms of different frequencies to investigate the coupled fluid flow and heat transfer behaviour. The numerical model was compared with published analytical studies and a good agreement was shown. At low frequencies, a hydrodynamic analysis indicated that since viscous forces are dominant, the wall shear, axial pressure gradient, and axial velocity profiles are all in phase. The pulsating friction factor followed the steady flow values closely. Thermal analysis indicated that since the thermal diffusion times scales were shorter, significant heat diffused from wall to fluid, overall leading to an increase in the fluid temperature. This led to a reduction in heat transfer compared to steady flow.

At high frequencies, due to shorter fluid displacement times scales, a phase lag developed between the axial pressure gradient and the velocity and wall shear profiles, reaching $\pi/2$ out of phase. A sharp rise in friction factor is observed due to increasing wall viscous effects. Flow reversal effects were noticed in near wall regions of the axial velocity profiles due to increased intensity of viscous effects. Since convection heat transfer remained dominant, the wall and bulk temperatures reduced with a subsequent increase in phase lag. The effects of wall heat diffusion dampened out and the heat transfer resembled a quasi-steady behaviour. The periodic symmetric characteristics of the imposed sinusoidal flow pulsation waveform results in a cyclic process of heat

removal and retention, which tends to attain a quasi-equilibrium state. The overall time averaged heat transfer for the pulsating flow is less than the steady flow and the thermal performance is $\eta < 1$. The highest thermal performance was obtained for $Wo = 5.1$. There is a potential heat transfer enhancement at higher flow rate amplitudes.

The aim of future studies shall be to investigate the heat transfer performance in the moderate frequency range using modulated sinusoidal pulsation waveforms.

Declaration of competing interest

The authors declare the following financial interests/personal relationships which may be considered as potential competing interests: Parth Kumavat reports a relationship with University of Dublin, Trinity College that includes: funding grants and travel reimbursement.

Data availability

Data will be made available on request.

Acknowledgements

The authors would like to thank Trinity College, University of Dublin, Ireland, for their financial support as well as Prof. Darina Murray for her guidance. We are grateful to the Trinity College Centre for High Performance Computing (TCHPC) and the Irish Centre for High End Computing (ICHEC) for their support and facilities to aid the numerical study.

Appendix A. Supplementary data

Supplementary material related to this article can be found online at https://doi.org/10.1016/j.ijthermalsci.2022.107790.

References

[1] T. Walsh, K. Yang, V. Nee, Q. Liao, Forced convection cooling in microelectronic cabinets via oscillatory flow techniques, Exp. Heat Transf. Fluid Mech. Thermodyn. (1993) 641–648, http://dx.doi.org/10.1016/b978-0-444-81619-1.50076-9.

[2] B. Mehta, S. Khandekar, Local experimental heat transfer of single-phase pulsating laminar flow in a square mini-channel, Int. J. Therm. Sci. 91 (2015) 157–166, http://dx.doi.org/10.1016/j.ijthermalsci.2015.01.008.

[3] Q.D. Liao, K.T. Yang, V.W. Nee, An analysis of conjugate heat transfer from a heated wall in a channel with zero-mean oscillatory flow for small oscillatory flow Reynolds numbers, Int. J. Heat Mass Transfer 37 (SUPPL. 1) (1994) 415–423, http://dx.doi.org/10.1016/0017-9310(94)90041-8.

[4] T. Moschandreou, M. Zamir, Heat transfer in a tube with pulsating flow and constant heat flux, Int. J. Heat Mass Transfer 40 (10) (1997) 2461–2466, http://dx.doi.org/10.1016/S0017-9310(96)00266-9.

[5] T. Persoons, T. Saenen, T. Van Oevelen, M. Baelmans, Effect of flow pulsation on the heat transfer performance of a minichannel heat sink, J. Heat Transfer 134 (9) (2012) 091702–1–091702–7, http://dx.doi.org/10.1115/1.4006485.

[6] D. Yin, H.B. Ma, Analytical solution of heat transfer of oscillating flow at a triangular pressure waveform, Int. J. Heat Mass Transfer 70 (2014) 46–53, http://dx.doi.org/10.1016/j.ijheatmasstransfer.2013.10.016.

[7] H.W. Cho, J.M. Hyun, Numerical solutions of pulsating flow and heat transfer characteristics in a pipe, Int. J. Heat Fluid Flow 11 (4) (1990) 321–330, http://dx.doi.org/10.1016/0142-727X(90)90056-H.

[8] R. Blythman, T. Persoons, N. Jeffers, D.B. Murray, Heat transfer of laminar pulsating flow in a rectangular channel, Int. J. Heat Mass Transfer 128 (2019) 279–289, http://dx.doi.org/10.1016/j.ijheatmasstransfer.2018.08.109.

[9] E.G. Richardson, The amplitude of sound waves in resonators, Proc. Phys. Soc. 40 (1) (1927) 206–220, http://dx.doi.org/10.1088/0959-5309/40/1/328.

[10] E.G. Richardson, E. Tyler, The transverse velocity gradient near the mouths of pipes in which an alternating or continuous flow of air is established, Proc. Phys. Soc. 42 (1) (1929) 1–15, http://dx.doi.org/10.1088/0959-5309/42/1/302.

[11] D.B. Holmes, J.R. Vermeulen, Velocity profiles in ducts with rectangular cross sections, Chem. Eng. Sci. 23 (7) (1968) 717–722, http://dx.doi.org/10.1016/0009-2509(68)85006-7.

[12] J. Harris, G. Peev, W.L. Wilkinson, Velocity profiles in laminar oscillatory flow in tubes, J. Phys. E: Sci. Instrum. 2 (11) (1969) 913–916, http://dx.doi.org/10.1088/0022-3735/2/11/301.

[13] C. Fan, B.T. Chao, Unsteady, laminar, incompressible flow through rectangular ducts, Z. Angew. Math. Phys. ZAMP 16 (3) (1965) 351–360, http://dx.doi.org/10.1007/BF01591915.

[14] J.R. Womersley, Method for the calculation of velocity, rate of flow and viscous drag in arteries when the pressure gradient is known, J. Physiol. 127 (3) (1955) 553–563, http://dx.doi.org/10.1113/jphysiol.1955.sp005276.

[15] T. Sexl, Über den von E. G. Richardson entdeckten "Annulareffekt", Z. Phys. 61 (5–6) (1930) 349–362, http://dx.doi.org/10.1007/BF01340631.

[16] R. Zengerle, J. Ulrich, S. Kluge, M. Richter, A. Richter, A bidirectional silicon micropump, Sensors and Actuators A: Physical 50 (1-2) (1995) 81–86, http://dx.doi.org/10.1016/0924-4247(96)80088-4.

[17] R.G. Lingford, N.W. Ryan, Pulsatile flow in rigid tubes, J. Appl. Physiol. 20 (5) (1965) 1078–1082, http://dx.doi.org/10.1152/jappl.1965.20.5.1078.

[18] E.B. Denison, W.H. Stevenson, Oscillatory flow measurements with a directionally sensitive laser velocimeter, Rev. Sci. Instrum. 41 (10) (1970) 1475–1478, http://dx.doi.org/10.1063/1.1684313.

[19] K. Haddad, O. Ertunç, M. Mishra, A. Delgado, Pulsating laminar fully developed channel and pipe flows, Phys. Rev. E (3) 81 (1) (2010) 1–13, http://dx.doi.org/10.1103/PhysRevE.81.016303.

[20] B. Ünsal, S. Ray, F. Durst, O. Ertunç, Pulsating laminar pipe flows with sinusoidal mass flux variations, Fluid Dyn. Res. 37 (5) (2005) 317–333, http://dx.doi.org/10.1016/j.fluiddyn.2005.06.002.

[21] F. Durst, U. Heim, B. Ünsal, G. Kullik, Mass flow rate control system for time-dependent laminar and turbulent flow investigations, Meas. Sci. Technol. 14 (7) (2003) 893–902, http://dx.doi.org/10.1088/0957-0233/14/7/301.

[22] M. Omhi, M. Iguchi, T. Usui, Flow pattern and frictional losses in pulsating pipe flow: Part 5 wall shear and flow pattern in a Laminar flow, Bull. JSME 24 (187) (1981) 75–81, http://dx.doi.org/10.1299/jsme1958.24.75.

[23] C. Aygun, O. Aydin, Hydrodynamics of piston-driven laminar pulsating flow: Part 2. Fully developed flow, Nucl. Eng. Des. 274 (2014) 172–180, http://dx.doi.org/10.1016/j.nucengdes.2014.02.018.

[24] R. Blythman, T. Persoons, N. Jeffers, K.P. Nolan, D.B. Murray, Localised dynamics of laminar pulsatile flow in a rectangular channel, Int. J. Heat Fluid Flow 66 (2017) 8–17, http://dx.doi.org/10.1016/j.ijheatfluidflow.2017.05.006.

[25] P.C. Chatwin, The approach to normality of the concentration distribution of a solute in a solvent flowing along a straight pipe, J. Fluid Mech. 43 (2) (1970) 321–352, http://dx.doi.org/10.1017/S0022112070002409.

[26] G. Taylor, Dispersion of soluble matter in solvent flowing slowly through a tube, Proc. R. Soc. A 219 (1137) (1953) 186–203, http://dx.doi.org/10.1098/rspa.1953.0139.

[27] O. Mamoru, K. Akira, Lumped-parameter modeling of heat transfer enhanced by sinusoidal motion of fluid, Int. J. Heat Mass Transfer 34 (12) (1991) 3083–3095, http://dx.doi.org/10.1016/0017-9310(91)90078-S.

[28] E.M. Sparrow, F.N. De Farias, Unsteady heat transfer in ducts with time-varying inlet temperature and participating walls, Int. J. Heat Mass Transfer 11 (5) (1968) 837–853, http://dx.doi.org/10.1016/0017-9310(68)90128-2.

[29] Y.K. Seo, H.K. Byung, M.H. Jae, Heat transfer in the thermally developing region of a pulsating channel flow, Int. J. Heat Mass Transfer 36 (17) (1993) 4257–4266, http://dx.doi.org/10.1016/0017-9310(93)90088-N.

[30] R. Siegel, M. Perlmutter, Heat transfer for pulsating laminar duct flow, J. Heat Transfer 84 (2) (1962) 111–122, http://dx.doi.org/10.1115/1.3684307.

[31] C. Xu, S. Xu, Z. Wang, D. Fenga, Experimental investigation of flow and heat transfer characteristics of pulsating flows driven by wave signals in a microchannel heat sink, Int. Commun. Heat Mass Transfer 125 (2021) 105343, http://dx.doi.org/10.1016/j.icheatmasstransfer.2021.105343.

[32] J. McEvoy, S. Alimohammadi, T. Persoons, Experimental investigation of flow pulsation waveforms in rectangular mesochannels for high heat flux electronics cooling, Exp. Therm Fluid Sci. 109 (December 2018) (2019) 109885, http://dx.doi.org/10.1016/j.expthermflusci.2019.109885.

[33] H. Zhang, S. Li, J. Cheng, Z. Zheng, X. Li, F. Li, Numerical study on the pulsating effect on heat transfer performance of pseudo-plastic fluid flow in a manifold microchannel heat sink, Appl. Therm. Eng. 129 (2018) 1092–1105, http://dx.doi.org/10.1016/j.applthermaleng.2017.10.124.

[34] F. Zhang, Y. Bian, Y. Liu, J. Pan, Y. Yang, H. Arima, Experimental and numerical analysis of heat transfer enhancement and flow characteristics in grooved channel for pulsatile flow, Int. J. Heat Mass Transfer 141 (2019) 1168–1180, http://dx.doi.org/10.1016/j.ijheatmasstransfer.2019.06.100.

[35] N. Kurtulmuş, B. Sahin, Experimental investigation of pulsating flow structures and heat transfer characteristics in sinusoidal channels, Int. J. Mech. Sci. 167 (October 2019) (2020) 105268, http://dx.doi.org/10.1016/j.ijmecsci.2019.105268.

[36] U. Akdag, S. Akcay, D. Demiral, Heat transfer enhancement with laminar pulsating nanofluid flow in a wavy channel, Int. Commun. Heat Mass Transfer 59 (2014) 17–23, http://dx.doi.org/10.1016/j.icheatmasstransfer.2014.10.008.

[37] S. Singh, S.K. Singh, H.S. Mali, R. Dayal, Numerical investigation of heat transfer in structured rough microchannels subjected to pulsed flow, Appl. Therm. Eng. 197 (July) (2021) 117361, http://dx.doi.org/10.1016/j.applthermaleng.2021.117361.

[38] P.S. Kumavat, R. Blythman, D.B. Murray, S.M. O'Shaughnessy, Study of heat transfer enhancement by pulsating flow in a rectangular mini channel, in: C. Wen, Y. Yan (Eds.), Advances in Heat Transfer and Thermal Engineering, Springer Singapore, Singapore, 2021, pp. 253–257, http://dx.doi.org/10.1007/978-981-33-4765-6_44.

[39] P. Kumavat, S.M. O'Shaughnessy, Experimental investigation of heat transfer enhancement by pulsating flow in a minichannel, J. Phys. Conf. Ser. 2116 (1) (2021) 012031, http://dx.doi.org/10.1088/1742-6596/2116/1/012031.

[40] S. Ray, B. Ünsal, F. Durst, O. Ertunc, O.A. Bayoumi, Mass flow rate controlled fully developed laminar pulsating pipe flows, J. Fluids Eng. Trans. ASME 127 (3) (2005) 405–418, http://dx.doi.org/10.1115/1.1906265.

[41] F. Durst, S. Ray, B. Ünsal, O.A. Bayoumi, The development lengths of laminar pipe and channel flows, J. Fluids Eng. 127 (6) (2005) 1154, http://dx.doi.org/10.1115/1.2063088.

[42] S.M. O'Shaughnessy, A.J. Robinson, The influence of the magnitude of gravitational acceleration on Marangoni convection about an isolated bubble under a heated wall, Heat Transf. Eng. 30 (13) (2009) 1096–1107, http://dx.doi.org/10.1080/01457630902922251.

[43] A.D. Canonsburg, ANSYS CFX-Solver Modeling Guide (August), 2017.

[44] P.K. Kundu, I.M. Cohen, D.R. Dowling, Fluid Mechanics, Academic Press, 2015, http://dx.doi.org/10.1016/C2012-0-00611-4.

[45] S. Alimohammadi, D.B. Murray, T. Persoons, On the numerical-experimental analysis and scaling of convective heat transfer to pulsating impinging jets, Int. J. Therm. Sci. 98 (2015) 296–311, http://dx.doi.org/10.1002/9781118032428.

[46] I.B. Celik, U. Ghia, P.J. Roache, C.J. Freitas, H. Coleman, P.E. Raad, Procedure for estimation and reporting of uncertainty due to discretization in CFD applications, J. Fluids Eng. Trans. ASME 130 (7) (2008) 0780011–0780014, http://dx.doi.org/10.1115/1.2960953.

[47] J. Majdalani, Exact Navier-Stokes solution for pulsatory viscous channel flow with arbitrary pressure gradient, J. Propul. Power 24 (6) (2008) 1412–1423, http://dx.doi.org/10.2514/1.37815.

[48] S. Uchida, The pulsating viscous flow superposed on the steady laminar motion of incompressible fluid in a circular pipe, Z. Angew. Math. Phys. ZAMP 7 (5) (1956) 403–422, http://dx.doi.org/10.1143/JPSJ.19.117.

[49] M. Ojha, R.L. Hummel, S.C. Cobbold, K.W. Johnston, Development and evaluation of a high resolution photochromic dye method for pulsatile flow studies, J. Phys. E: Sci. Instrum. 21 (10) (1988) 998–1004, http://dx.doi.org/10.1088/0022-3735/21/10/018.

[50] D.E. Muntges, J. Majdalani, Pulsatory channel flow for an arbitrary volumetric flowrate, in: 32nd AIAA Fluid Dynamics Conference and Exhibit (June), 2002, pp. 1–8, http://dx.doi.org/10.2514/6.2002-2856.

[51] H. Yuan, S. Tan, N. Zhuang, L. Tang, Theoretical analysis of wall thermal inertial effects on heat transfer of pulsating laminar flow in a channel, Int. Commun. Heat Mass Transfer 53 (2014) 14–17, http://dx.doi.org/10.1016/j.icheatmasstransfer.2014.02.003.

[52] H.N. Hemida, M.N. Sabry, A. Abdel-Rahim, H. Mansour, Theoretical analysis of heat transfer in laminar pulsating flow, Int. J. Heat Mass Transfer 45 (2002) 1767–1780, http://dx.doi.org/10.1016/S0017-9310(01)00274-5.

[53] G.J. Brereton, Y. Jiang, Convective heat transfer in unsteady laminar parallel flows, Phys. Fluids 18 (10) (2006) 103602, http://dx.doi.org/10.1063/1.2359742.